A Next-Generation In-Situ Nanoprobe Beamline for the Advanced Photon Source

Jörg Maser,[a] Barry Lai,[a] Tonio Buonassisi,[b] Zhonghou Cai,[a] Si Chen,[a] Lydia Finney,[a] Sophie-Charlotte Gleber,[a] Ross Harder,[a] Chris Jacobsen,[a] Wenjun Liu, [a] Conal Murray,[c] Curt Preissner,[a] Chris Roehrig,[a] Volker Rose,[a] Deming Shu,[a] David Vine,[a] Stefan Vogt.[a]

[a]Argonne National Laboratory, Argonne, IL, United States; [b]Massachusetts Institute of Technology, Cambridge, MA, USA; [c]IBM T.J. Watson Research Center, Yorktown Heights, NY USA.

ABSTRACT

The Advanced Photon Source is currently developing a suite of new hard x-ray beamlines, aimed primarily at the study of materials and devices under real conditions. One of the flagship beamlines of the APS Upgrade is the In-Situ Nanoprobe beamline (ISN beamline), which will provide *in-situ* and *operando* characterization of advanced energy materials and devices under change of temperature and gases, under applied fields, in 3D.

The ISN beamline is designed to deliver spatially coherent x-rays with photon energies between 4 keV and 30 keV to the ISN instrument. As an x-ray source, a revolver-type undulator with two interchangeable magnetic structures, optimized to provide high brilliance throughout the range of photon energies of 4 keV – 30 keV, will be used. The ISN instrument will provide a smallest hard x-ray spot of 20 nm using diffractive optics, with sensitivity to sub-10 nm sample structures using coherent diffraction. Using nanofocusing mirrors in Kirkpatrick-Baez geometry, the ISN will also provide a focus of 50 nm with a flux of $8 \cdot 10^{11}$ Photons/s at a photon energy of 10 keV, several orders of magnitude larger than what is currently available. This will allow imaging of trace amounts of most elements in the periodic table, with a sensitivity to well below 100 atoms for most metals in thin samples. It will also enable nano-spectroscopic studies of the chemical state of most materials relevant to energy science. The ISN beamline will be primarily used to study inorganic and organic photovoltaic systems, advanced batteries and fuel cells, nanoelectronics devices, and materials and systems designed to reduce the environmental impact of combustion.

Keywords: x-ray, nanofocusing, x-ray nanoprobe, energy science, materials science, x-ray optics

1. INTRODUCTION

Hard X-ray nanoprobes have been developed to bring to bear the unique properties of hard x-rays to nanoscale studies of hard and soft materials, devices, and biological as well as environmental systems.[1,2,3,4,5,6,7] Hard x-rays combine high penetration with exquisite trace element sensitivity, the capacity to probe the phase and structure of crystalline materials, while being non-destructive and being unaffected by magnetic and electric fields. Modern storage rings provide partially coherent hard x-rays, which can be manipulated into fully coherent beams with very high photon flux. Such beams allow diffraction-limited focusing of hard x-rays to spot sizes only limited by the intrinsic properties of focusing x-ray optics, yielding x-ray probes with sizes close to 10 nm. Coherent x-rays allow in addition the deployment of coherent techniques such as holography, coherent imaging and ptychography, which can be used to obtain x-ray images either without use of x-ray optics, or, when using focusing optics, to increase the contrast of sample features with dimensions smaller than the focal spot size and achieve sub-spot size resolution. As such, nanofocused hard x-rays bring x-ray techniques such as x-ray fluorescence imaging, spectroscopy, x-ray diffraction and x-ray scattering to the scale of inhomogeneities, individual defects and active sites that are intrinsic to most materials, to biological systems and to advanced nanoscale devices.

As part of the Upgrade of the Advanced Photon Source, we are developing the In-Situ Nanoprobe (ISN) beamline,[8] a next-generation hard x-ray nanoprobe that utilizes advances in nanofocusing x-ray optics, advanced positioning and controls capabilities towards the study of materials and devices under *in-situ* and *operando* conditions. Advanced

X-Ray Nanoimaging: Instruments and Methods, edited by Barry Lai, Proc. of SPIE Vol. 8851, 885106

materials and devices such as organic and inorganic photovoltaic systems, batteries and fuel cells, nanoscale electronics, as well as biological samples and complex environmental systems, are often characterized by inhomogeneities on many length scales, with nanoscale features and defects that can affect or even determine the macroscopic performance and behavior of these systems. To probe such small defects while maintaining multi-length scale imaging capabilities, the ISN combines reflective and diffractive nanofocusing optics. Nanofocusing mirrors in Kirkpatrick-Baez (K-B) geometry will be used to focus coherent x-rays into a diffraction-limited spot of 50 nm.[9,10] Diffractive optics such as Fresnel zone plates (ZPs) or multilayer Laue lenses (MLLs) will be used to focus x-rays into a spot of 20 nm.[11,12,13] The ISN will deploy a variety of *in-situ* specimen cartridges to provide temperatures between 40 K and 1300 K, allow flow of gases and fluids, and/or apply external fields. The ISN will be capable of measuring voltages and currents *in-* and *operando*, and deploy added detection modes such as x-ray beam induced current (XBIC). The main contrast mechanism will be x-ray fluorescence imaging and spectroscopy, which allows measurement and quantification of the 2D and 3D distribution of elemental and chemical species, with a sensitivity to less than 100 atoms for most metals. A secondary contrast mechanism is based on ptychography, and will allow imaging of the structure of transparent samples at a spatial resolution well below the focal spot size.[14,15] The ISN beamline will use x-rays with photon energies between 4 keV and 30 keV, enabling x-ray imaging and x-ray spectroscopy for most elements in the periodic table.

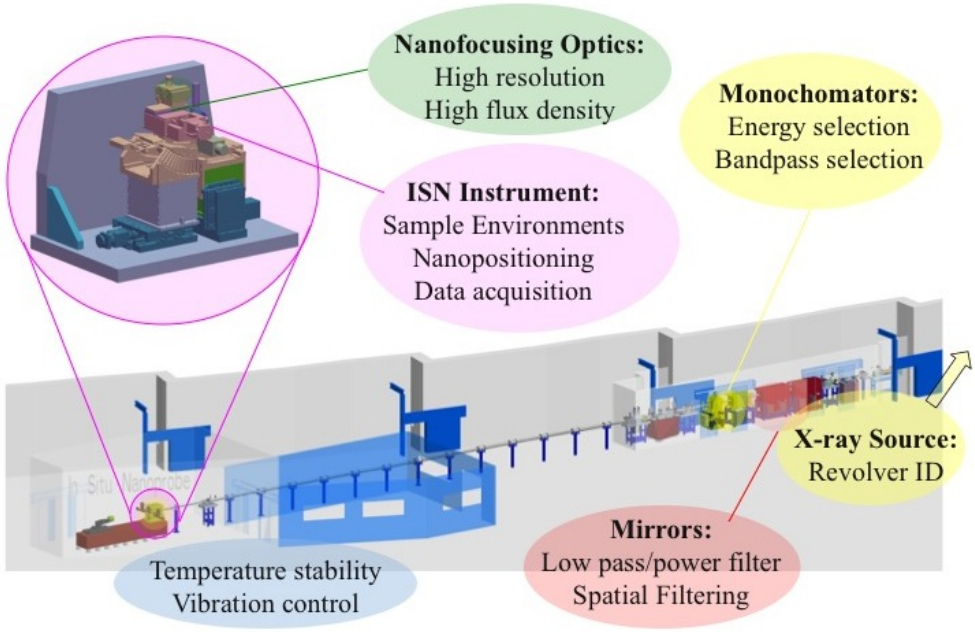

Figure 1. Layout of the ISN beamline. A revolver-type undulator with a length of 2.4 m and periods of 3.3 cm and 2.7 cm, respectively, provides a tunable hard x-ray beam with high brilliance. The upstream section of the beamline (to the right in Fig. 1) houses masks and slits, high-power mirrors for harmonics rejection and intermediate focusing, and two monochromators with bandpath of $\Delta E/E = 10^{-2}$ and $\Delta E/E = 10^{-4}$, respectively. The downstream section of the beamline (to the left of Fig. 1) houses a temperature-stabilized enclosure for the ISN instrument, with an anteroom and a controls room shielding the enclosure from temperature variations in the APS ring building. The ISN instrument contains nanofocusing optics, nanpositioners for optics and sample holders with a laser-interferometric feedback system, *in-situ* cartridges, detectors and and data acquisition systems.

Figure 1 shows the layout of the ISN beamline.[8] Intense, partially coherent x-rays from the insertion device inside the APS storage ring propagate into the First Optical Enclosure (FOE). In the FOE, high heatload mirrors are used for low-pass/power filtering of the undulator spectrum, for rejection of higher undulator harmonics, and to manipulate the x-ray beam to allow extraction of the spatially coherent fraction of the undulator beam. Monochromators are used for energy and bandwidth selection, with a double crystal monochromator (DCM) providing a bandpass of $\Delta E/E = 10^{-4}$, matched to the bandwidth requirements of diffractive optics and used for nanospectroscopy, and a double multilayer monochromator (DMM) providing a bandpass of $\Delta E/E = 10^{-2}$, for use with nanofocusing mirrors for elemental imaging. The monochromatized beam is focused into a secondary source on a beam defining aperture (BDA) positioned at 42.2 m from the source. The BDA selects a fully or partially coherent part of the undulator beam, which in turn propagates into

the ISN endstation. The ISN endstation houses the ISN instrument, which is positioned at 72 m from the x-ray source. The ISN instrument consists of a vibration-isolating support structure, nanofocusing x-ray optics, sample environments and related equipment, detectors, controls electronics, and auxiliary components. The endstation enclosure contains systems to stabilize the temperature to 0.1 K, and to minimize vibrations.

2. X-RAY SOURCE

The x-ray source is a revolver-type undulator with periods of 3.3 cm and 2.7 cm. This device provides hard x-rays with a brilliance of close to 10^{20} photons/s/mm^2/mrad^2/0.1% BW, yielding a coherent flux of $10^{11} – 10^{12}$ Photons/s/0.1%BW in the range of photon energies between 4 keV and 12 keV, and of 10^{10} Photons/s/0.1% BW at a photon energy of 30 keV. Figure 2 shows both the brilliance and the corresponding coherent flux for the 3.3 cm device.

The x-ray source is characterized by the following parameters:

Electron and photon beam properties for a photon energy of 10 keV	
Electron beam parameters	X-ray beam parameters
$\sigma_x = 274.3$ µm	$\Sigma_x = 274.3$ µm
$\sigma_y = 10.3$ µm	$\Sigma_y = 11.0$ µm
$\sigma'_x = 11.27$ µrad	$\Sigma'_x = 12.4$ µrad
$\sigma'_y = 3.58$ µrad	$\Sigma'_y = 6.3$ µrad

where' $\Sigma_{x,y}' = (\sigma_{x,y}^2 + \sigma_r^2)^{1/2}$ and $\Sigma_{x,y}' = (\sigma_{x,y}^2 + \sigma_r'^2)^{1/2}$ and $\sigma_r = (2\lambda L)^{1/2}/4/\pi$, $\sigma_r' = (\lambda/(2L))^{1/2}$, with L the length of the undulator, and λ the x-ray wavelength.

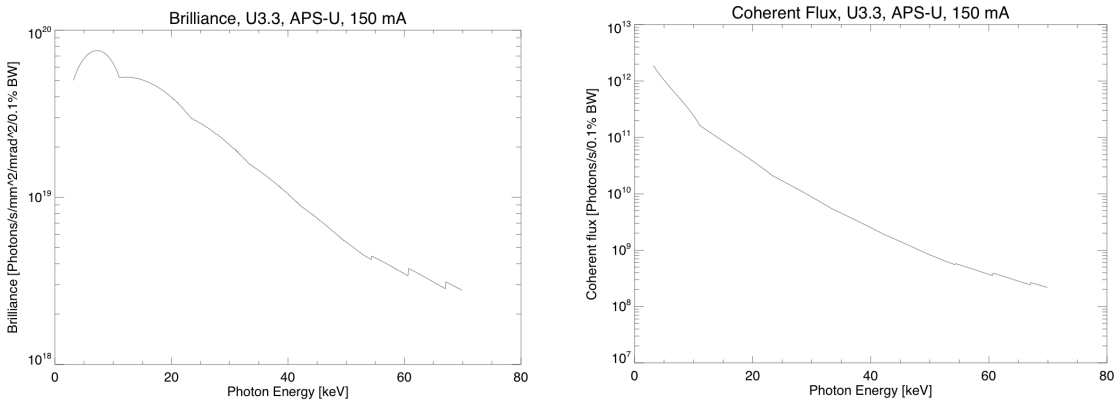

Figure 2. Brilliance (left) and coherent flux (right) versus photon energy, for an insertion device with a length of 2.4 m and period of 3.3 cm, at a synchrotron current of 150 mA. While the maximum brilliance is reached for photon energies between 5 keV and 12 keV, APS insertion devices provide high brilliance for photon energies of 50 keV and above using high undulator harmonics. For consistency purposes, both the brilliance and the coherent flux are expressed for a bandwidth of 0.1%. When operating with a DCM, the bandwidth used would be approximately 0.01%. When operating with a DMM, the bandwidth used would be approximately 1%.

3. NANOFOCUSING OPTICS

Several criteria are important in identifying nanofocusing optics for a particular purpose: the spatial resolution limit δ, the acceptance A, the bandwidth capability $\Delta E/E$, the chromaticity $f(E)$, the working distance, and the suitability for imaging of an extended field. Here, f indicates the focal length. Reflective, refractive and diffractive optics can all focus to spot sizes of 100 nm and below, and the trade-offs between the characteristics listed above determine the choice of nanofocusing optics for a specific instrument. The main considerations for the ISN beamline are: (i) very high spatial resolution to allow characterization of individual defects (ii) acceptance of the full lateral coherence length of the incident hard x-ray beam (iii) sufficient working distance to allow placement of *in-situ* specimen cells (iv) high flux to allow fast imaging across multiple length scales, in 3D and in 4D, and (v) non-dispersive focusing to enable x-ray fluorescence spectroscopy. No single optic is capable of delivering all of these requirements. Therefore, the ISN

instrument is designed to accommodate two different types of optics, a K-B mirror system capable of focusing to 50 nm, and diffractive optics for focusing to 20 nm or below. The K-B system is non-chromatic, and therefore allows acceptance of almost the full bandwidth of $\Delta E/E \sim 10^{-2}$ from a typical undulator source. This yields very high focused photon flux, enabling fast multi length-scale imaging, x-ray fluorescence tomography and 4D imaging. A K–B system does not require positioning of an order sorting aperture close to the focal spot, as do diffractive optics, thereby maximizing the working distance and the space for *in-situ* specimen cells. Due to absence of chromaticity, nano-spectroscopy can be performed without need to adjust the focal position. Diffractive optics, on the other hand, can provide highest spatial resolution at reasonable length of a beamline (50 – 200 m), are compact along the optical axis as well as in the beam plane, and are light. Both K-B systems and diffractive optics can be fabricated with dimensions that allow acceptance of the full lateral coherence length of a typical undulator beamline of several 100 μm, and have, for spot sizes of 10 nm and above, uniform pupil functions without limitation of the effective aperture. Use of such a combination of K-B optics and diffractive optic combines highest spatial resolution of 20 nm or below with very high focused flux and full spectroscopy at somewhat reduced resolution.

3.1 Reflective Nanofocusing Optics

Elliptically figured mirrors in K-B geometry will be used to focus monochromatic hard x-rays into a diffraction-limited spot on the sample. The nanofocusing mirror system (NMS) will accept x-rays with photon energies between 4 keV and 30 keV, with a bandpass of 10^{-2} using a DMM, or of 10^{-4} using a DCM. To achieve a diffraction-limited spot size of δ_R, mirrors must have sufficient length to subtend the numerical aperture defined by: $NA = 0.44\lambda/\delta_R$. At the same time, the demagnification must be sufficient such that the geometrical-optics image of the source, B, is significantly smaller than the diffraction-limited spot size, and slope errors must be sufficiently small.

In identifying the parameters for a NMS with a focal spot size of 50 nm, the diffraction limit, the demagnification of the source, and slope errors of the mirror substrates must be taken into account. We hereby assume that the mirror figure is an accurate ellipse. To define the parameters of the NMS, we use the following expression:

$$\delta = \sqrt{[(0.44 \cdot \lambda / NA)^2 + (2.35 \cdot \sigma_{Sc} \cdot M)^2 + (2.35 \cdot \sigma_{Sl} \cdot f)^2]}, \quad (1)$$

where δ is the spot size, λ the x-ray wavelength, σ_{SC} the source size, M the magnification ($M << 1$), σ_{Sl} the slope error, and f the focal length. All individual terms of the sum are assumed to be Gaussian, and scaled to full-width at half maximum (FWHM), yielding an expression for the FWHM spot size. From eq. (1), it is clear that the focal length must be small to achieve large demagnification $1/M$, and that the numerical aperture must be large enough to yield a diffraction-limited spot size of well below 50 nm.

The mirror system will be positioned at a distance of 72 m from the source, and be illuminated from the secondary aperture 42.2 m from the source. The horizontally focusing mirror (HFM) is positioned in the downstream position, the vertically focusing mirror (VFM) in the upstream position. Both mirrors are positioned at a grazing angle of 2.5 mrad, yielding good reflectivity for up to 32 keV for a platinum coating. We chose a length of 60 mm and a focal length of 60 mm for the HFM. The mirror will accept a lateral beam size of 150 μm, corresponding to the lateral coherence length at 10 keV. The HFM yields a diffraction-limited spot size of 33 nm, and a magnification of 1/500. For spatially coherent illumination of the HFM at a photon energy of 10 keV, the secondary aperture must be closed to a size of 10.7 μm, yielding a demagnified spot size B of 21 nm. For a slope error of 0.1 μrad, the expression (1) yields a horizontal spot size of 39.7 nm, which is sufficiently small to allow for added errors, such as edge effects and imperfect figure, and still remain at or below a spot size 50 nm. For the VFM, we chose a length of 175 mm, and a focal length of 180 mm. In this configuration, the mirror provides the same numerical aperture as the HFM, and thereby the same diffraction limit. The mirror will accept a lateral beam size of 450 μm. For coherent illumination, the secondary source must be closed to a very small vertical size of 4 μm, which in turn necessitates intermediate focusing in the vertical direction, upstream of the secondary aperture. The magnification by the VFM is 1/165, yielding a demagnified spot size of 24 nm. Due to the long focal length, very small slope errors are desired. For a slope error of 0.035 μrad, the vertical spot size is 40.8 nm; the spot size for slope errors of 0.1 μrad would be 44.6 nm, still consistent with the goal of a 50 nm spot, but with less tolerance to added errors.

3.2 Diffractive Nanofocusing Optics

While nanofocusing mirrors can today be fabricated with figure errors and slope errors sufficient to achieve a spatial resolution of below 10 nm in one dimension, multilayer coatings or a very long beamline are required to deploy such

optics. The ISN will therefore use diffractive optics to achieve a focal spot size of 20 nm. Such optics require a smallest structure size of 15 nm across typical apertures of 100 μm- 300 μm, and thickness along the optical axis in the range of hundreds of nanometers to many micrometers. ZPs are very well suited for imaging and focusing of x-rays with high spatial resolution. However, due to the technical challenges of fabricating the high aspect ratios required for efficient focusing of x-rays with photon energies above 15 keV, ZPs are best suited for use at lower photon energies. Multilayer-based diffractive optics such as MLLs have demonstrated high diffraction efficiency and excellent resolution at photon energies of 12 keV and above,[13] and are an alternate approach for focusing hard x-rays to a small spot. Figure 4 shows the calculated diffraction efficiency of ZPs with an outermost zone width of 15 nm,[16] and of 2D focusing MLLs with smallest structures between 5 nm and 8 nm.[17] ZPs with an outermost zone with of ~ 25 nm and a thickness of 0.5 μm can be fabricated today. A factor t in thickness and corresponding efficiency gain can routinely be achieved by stacking two ZPs in close proximity. On the other hand, MLLs with structures as small as 4 nm in flat geometry can be fabricated today, and MLL optics with increasing acceptance are being fabricated.[18] To achieve very high efficiency at high photon energies, wedged ("Bragg") MLLs are under development.

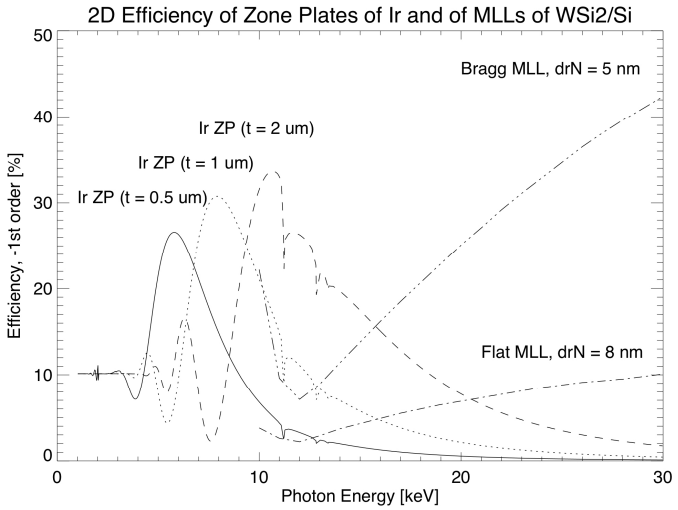

Figure 3. Calculated 2D diffraction efficiency of ZPs of iridium and of MLLs of WSi_2/Si, for photon energies between 1 keV and 30 keV. Parameters for ZPs are chosen to yield a spot size of 20 nm, with an outermost zone width dr_N of 15 nm. Parameters for MLLs are chosen to yield a spot size in the range of 5 nm – 20 nm, depending on the acceptance of the MLL. The ZPs do not exhibit dynamical diffraction effects; the MLLs are designed to take advantage of dynamic diffraction effects by use of small d-spacings and high aspect ratios. The efficiency of ZPs is plotted for fixed thicknesses of 0.5 μm, 1 μm and 2 μm. The efficiency of MLLs with optimized thickness is plotted for two different geometries, flat MLLs, where the Bragg condition is satisfied only locally, and wedged MLLs ("Bragg-MLL"), where the Bragg condition is satisfied across the aperture of the MLL. In each case, two MLLs are positioned consecutively for vertical and horizontal focusing. The thickness and thereby the efficiency of ZPs is limited by the highest aspect ratios that can be fabricated, making ZPs an excellent optic for the low and possibly intermediate range of photon energies. For energies above 15 keV, the focusing efficiency even of very high-aspect ratio ZPs rapidly decreases; at the same time, the efficiency of MLLs increases with photon energy, with the 2D efficiency of wedged MLLs capable of achieving more than 40% at a photon energy of 30 keV.

4. SUMMARY

The ISN beamline is one of the flagship beamlines being developed as part of the Upgrade of the Advanced Photon Source. The ISN is designed to allow study of energy materials and devices under *in-situ* and *operando* conditions. Using reflective optics, the ISN will provide a very high photon flux of $7 \cdot 10^{11}$ Photons/s at a bandwidth of 1% into a spot of 50 nm, for a photon energy of 10 keV. Diffractive optics will provide a photon flux of $4 \cdot 10^{9}$ Photons/s at a bandwidth of 0.01% into a focal spot of 20 nm, at 10 keV. The primary contrast mechanism is x-ray fluorescence imaging and x-ray fluorescence spectroscopy. Coherent diffraction and ptychography in small-angle geometry will be performed in parallel to x-ray fluorescence, and allow to detect sample features with a size of well below 10 nm, with a sensitivity of less than 100 atoms. The ISN will provide a variety of *in-situ* environments, including cooling to 40 K, heating to 1300 K, flow of inert and reactive gases

and fluids, and application of electric fields. The ISN will study inorganic and organic photovoltaic systems, batteries, fuel cells, nanoelectronic devices, and systems relevant for CO_2 reduction and sequestration, such as geopolymers and cement.

5. ACKNOWLEDGMENTS

We thank O. Schmidt for his help in beamline design work, R. Dejus for preparing tuning curves for the ISN undulator, and L. Assoufid for his suggestions on x-ray mirrors. We furthermore thank our colleagues S. Darling, T. Rajh, W. Chiu, K. Kemner, P. Monteiro, E. Ingall, Y. Chu and H. Yan for valuable scientific and technical discussions, and their continued engagement in the ISN facility. T.B. acknowledges funding from U.S. Department of Energy SunShot Initiative under Contracts No. DE-EE0005314, DE-EE0005329, and DE-EE0005948. Use of the Advanced Photon Source (APS) at Argonne National Laboratory was supported by the U.S. Department of Energy, Office of Science, Office of Basic Energy Sciences, under Contract No. DE-AC02-06CH11357.

REFERENCES

[1] J. Maser, R. P. Winarski, M. Holt, D. Shu, C. Benson, B. Tieman, C. Preissner, A. Smolyanitskiy, B. Lai, S. Vogt, G. Wiemerslage, G. B. Stephenson: *Proc. 8th Int. Conf. X-ray Microscopy, IPAP Conf. Series 7, 26-29.*
[2] S. Chen, C. Flachenecker, B. Lai, T. Paunesku, B. Hornberger, C. Roehrig, J. VonOsinski, M. Bolbat, J. Maser, D. Shu, L. Finney, S. Gleber, Q. Jin, K. Brister, C. Jacobsen, S. Vogt, and G. Woloschak: *Microscopy and Microanalysis, 2012, vol 18 (S2), 962-963.*
[3] R. P. Winarski, M. V. Holt, V. Rose, P. Fuesz, D. Carbaugh, C. Benson, D. Shu, D. Kline, G. B. Stephenson, I. McNulty, J. Maser: *J. Synchrotron Rad., 2013, vol. 19 (6), 1056-1060.*
[4] C. G. Schroer, P. Boye, J. M. Feldkamp, J. Patommela, D. Samberg, A. Schropp, A. Schwab, S. Stephan, G. Falkenberg, G. Wellenreuther, N. Reimers: *Nucl. Instrum. Methods, Phys. Res. A, 2010, vol. 616, 93.*
[5] P. Bleuet, P. Cloetens, P. Gergaud, D. Mariolle, N. Chevalier, R. Tucoulou, J. Susini, and A. Chabli: *Rev. Sci. Instrum. 2009, vol. 80, 056101.*
[6] A. Somogyi, C. M. Kewish, F. Polack, and T. Moreno: *AIP Conf. Proc., 2011. 1365, pp. 57-60.*
[7] Y. S. Chu: *Preliminary Design Report for the Hard X-ray (HXN) Nanoprobe Beamline. National Synchrotron Light Source II, Brookhaven National Laboratory, LT-C-XFD-HXN-PDR-001, (2010).*
[8] J. Maser, B. Lai, T. Buonassisi, Z. Cai, S Chen, L. Finney, S.C. Gleber, C. Jacobsen, C. Preissner, C. Roehrig, V. Rose, D. Shu, D. Vine, S. Vogt. Metall. Mater. Trans. A (2013): 1–14, DOI 10.1007/s11661-013-1901-x.
[9] H. Mimura, S. Handa, T. Kimura, H. Yumoto, D. Yamakawa, H. Yokoyama, S. Matsuyama, K. Inagaki, K. Yamamura, Y. Sano, K. Tamasaku, Y. Nishino, M. Yabashi, T. Ishikawa and K. Yamauchi: *Nat. Phys., 2009, 6(2), 122.*
[10] W. Liu, G. E. Ice, L. Assoufid, C. Liu, B. Shi, R. Khachatryan, J. Qian, P. Zschack, J. Z. Tischler and J.-Y. Choi: *J. Synchrotron Rad., 2011, vol. 18(4), 575–579.*
[11] J. Vila-Comamala, Y. Pan, J. Lombardo, W. M. Harris, W. K. Chiu, C. David and Y. Wang: *J. Synchrotron Rad. (2012), vol. 19, 705-709.*
[12] J. Vila-Comamala, S. Gorelick, E. Färm, C. M. Kewish, A. Diaz, R. Barrett, V. A. Guzenko, M. Ritala, and C. David: *Opt. Express, 2011, vol. 19, 175 – 184.*
[13] H. Yan, V. Rose, D. Shu, E. Lima, H. C. Kang, R. Conley, C. Liu, N. Jahedi, A. T. Macrander, G. B. Stephenson, M. V. Holt, Y. S. Chu, M. Lu, J. Maser: *Opt. Express, 2011,vol.* 19 (16), 15069-15076.
[14] I. Peterson, B. Abbey, C.T. Putkunz, D.J. Vine, G.A. van Riessen, G.A. Cadenazzi, E. Balaur, R. Ryan, H.M. Quiney, I. McNulty, A.G. Peele, and K.A. Nugent: *Optics Express, 2012, vol. 20 (22), pp. 24678-24685.*
[15] D. J. Vine, D. Pelliccia, C. Holzner, S. B. Baines, A. Berry, I. McNulty, S. Vogt, A. G. Peele, and K. A. Nugent: *Optics Express, 2012, vol. 20 (16), pp. 18287-18296.*
[16] J. Kirz: *JOSA 64 (3), 1974, 301.*
[17] J. Maser, G. Schmahl: *Opt. Comm. 89 (2-4), 1992, 355.*
[18] R. Conley, N. Bouet, J. Zhou, H. Yan, Y. Chu, K. Lauer, J. Miller, L. Chub, Nima Jahedi: *Proc. of SPIE Vol. 8502, 2012, 850202-4.*